Systemic Inflammation and the Inflammatory Context of the Colonic Microenvironment Are Improved by Urolithin A

Marmar R. Moussa[1,2], Nuoxi Fan[1], John Birk[3], Anthony A. Provatas[4], Pratik Mehta[1], Yuichiro Hatano[1], Ock K. Chun[5], Manije Darooghegi Mofrad[5], Ali Lotfi[6], Alexander Aksenov[6], Vinicius N. Motta[7], Maryam Zenali[1,8], Haleh Vaziri[3], James J. Grady[9], Masako Nakanishi[1], and Daniel W. Rosenberg[1]

ABSTRACT

Diet affects cancer risk, and plant-derived polyphenols exhibit cancer-preventive properties. Walnuts are an exceptional source of polyphenolic ellagitannins, converted into urolithins by gut microflora. This clinical study examines the impact of urolithin metabolism on inflammatory markers in blood and colon polyp tissue. We evaluate the effects of walnut consumption on urinary urolithins, serum inflammatory markers, and immune cell markers in polyp tissues obtained from 39 subjects. Together with detailed food frequency data, we perform integrated computational analysis of metabolomic data combined with serum inflammatory markers and spatial imaging of polyp tissues using imaging mass cytometry. LC/MS-MS analyses of urine and fecal samples identify a widely divergent capacity to form nine urolithin metabolites in this patient population. Subjects with higher urolithin A formation exhibit lower levels of several key serologic inflammatory markers, including C-peptide, soluble form of intracellular adhesion molecule 1, sIL-6R, ghrelin, TRAIL, sVEGFR2, platelet-derived growth factor (PDGF), and MCP-2, alterations that are more pronounced in obese individuals for soluble form of intracellular adhesion molecule 1, epithelial neutrophil–activating peptide 78, leptin, glucagon-like peptide 1, and macrophage inflammatory protein 1δ. There is a significant increase in levels of peptide YY associated with urolithin A formation, whereas TNFα levels show an opposite trend, recapitulated in an *in vitro* system with ionomycin/phorbol 12-myristate 13-acetate–stimulated peripheral blood mononuclear cells (PBMC). Spatial imaging of colon polyp tissues shows altered cell cluster patterns, including a significant reduction of vimentin and CD163 expression associated with urolithin A. The ability to form urolithin A is linked to inflammation, warranting further studies to understand the role of urolithins in cancer prevention.

Prevention Relevance: We evaluate cancer-protective effects of walnuts via formation of microbe-derived urolithin A, substantiating their functional benefits on serum inflammatory markers and immunologic composition of polyps in normal/obese subjects. Our approach incorporates personalized nutrition within the context of colonic health, providing the rationale for dietary inclusion of walnut ellagitannins for cancer prevention.

Introduction

Walnuts are an exceptional source of phytochemicals, including pedunculagin, an ellagitannin that is hydrolyzed in the upper gastrointestinal (GI) tract, forming the non-flavonoid polyphenol ellagic acid (**Fig. 1A**; ref. 1). Ellagic acid is converted by the gut microbiome into a complex panel of urolithins (hydroxy-dibenzo[b,d]pyran-6-ones; ref. 2) that have gained traction in recent years for their health benefits in patients with chronic disorders, including obesity, cardiovascular diseases, and cancer (1). Extensive variability in urolithin metabolism is directly related to an individual's microbiome, although the bacteria responsible for each metabolic step are uncertain (2, 3). Urolithin A is of particular interest for its potent anticancer, anti-inflammatory, and prebiotic activities (1, 3) and most recently for its effects on T-cell activity (4, 5).

Our laboratory previously examined the effects of walnuts on mouse models of intestinal disease (6–9). Using the colon carcinogen azoxymethane, we tested the effects of walnuts added to Total Western Diet, formulated to model typical American intake of macro- and micronutrients and fat (10), and found a significant reduction in tumors in male mice consuming 7% walnuts (6). We identified a microbial signature directly associated with walnut ingestion and cancer

[1]Center for Molecular Oncology, School of Medicine, University of Connecticut, Farmington, Connecticut. [2]School of Computer Science, University of Oklahoma, Norman, Oklahoma. [3]Division of Gastroenterology, University of Connecticut, Farmington, Connecticut. [4]Center for Environmental Sciences and Engineering, University of Connecticut, Storrs, Connecticut. [5]Department of Nutritional Sciences, University of Connecticut, Storrs, Connecticut. [6]Department of Chemistry, University of Connecticut, Storrs, Connecticut. [7]Standard BioTools Canada Inc., Markham, Canada. [8]School of Public Health, University of Vermont, Burlington, Vermont. [9]Department of Public Health Sciences, University of Connecticut, Storrs, Connecticut.

M.R. Moussa and N. Fan contributed equally to this article.

Corresponding Author: Daniel W. Rosenberg, Center for Molecular Oncology, School of Medicine, University of Connecticut Health Center, 263 Farmington Avenue, Farmington, CT 06030. E-mail: rosenberg@uchc.edu

Cancer Prev Res 2025;18:235–50

doi: 10.1158/1940-6207.CAPR-24-0383

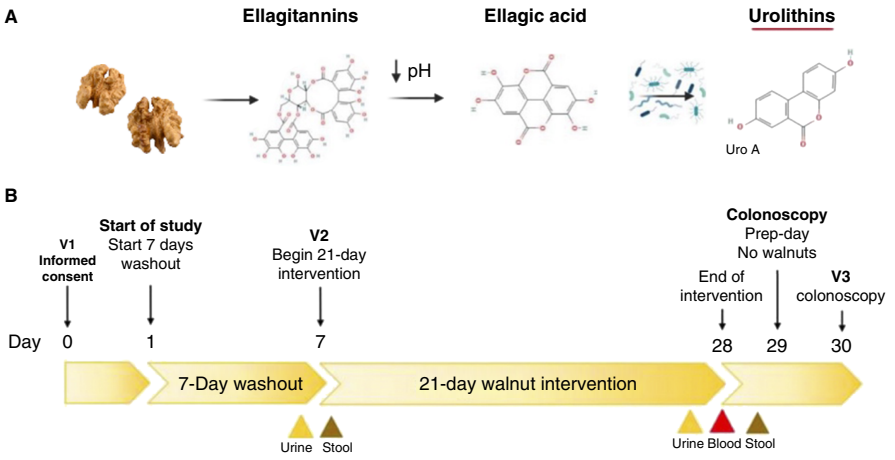

Figure 1.
Clinical study design. **A,** Overview of ellagitannin metabolism after ingestion. **B,** Overall study design. V, visit; Uro A, urolithin A.

suppression similar to that previously reported for inflammation-associated colorectal cancer (6, 11). Walnuts increased overall bacterial diversity in males, ultimately reaching levels comparable with females (6). Thus, it is possible that males underwent beneficial diet-induced changes in microbial composition that might contribute to an overall protective luminal environment. We recently identified three enterotype-like clusters associated with carcinogen exposure, walnut consumption, and Total Western Diet (9), providing further evidence that walnuts may modify colorectal cancer risk associated with Western diet by altering gut microbial composition.

This clinical study aims to validate the concept that important protective effects of walnuts occur through the formation of specific microbe-derived metabolites, in part through enhancing urolithin formation. We have substantiated the functional benefits of walnuts and defined the downstream consequences of human interindividual variability in urolithin metabolism. We have established correlations between urolithin formation and serum inflammatory markers. Additionally, the downstream consequences of urolithin formation in the composition of the tumor microenvironment (TME) in polyp tissue using high-dimensional spatial imaging are evaluated. Our approach has incorporated personalized nutrition within the context of colonic health, providing the rationale for incorporating dietary inclusion of walnut ellagitannins for cancer prevention.

Materials and Methods

Study design

The entire study design can be found in **Fig. 1B**. At visit 1, participants underwent a screening process to ensure eligibility. After consent, subjects began a 1-week run-in and were asked to stop taking dietary supplements, including probiotics, and to avoid consumption of walnuts and foods known to contain ellagic acid throughout the entire 4-week study period (Supplementary Table S1; ref. 12). Immediately following the 1-week run-in (baseline), participants were instructed to consume walnuts (56 g/day whole peeled) for 3 weeks. The walnut concentration selected was based on prior efficacy studies (13–15). At baseline and at the end of the dietary intervention, patients provided spot urine and fecal samples. Dietary records were used for compliance and to ensure that participants did not modify their dietary patterns during the study. An integrated computational analysis was undertaken, stratifying patients based on their levels of urolithin A and correlating these data with serum inflammatory markers. Spatial analysis of colon polyps was performed using imaging mass cytometry (IMC) at near single-cell resolution, contrasting low- and high-urolithin producers. This study was reviewed and approved by the University of Connecticut Health Center Institutional Review Board and Ethics Committee, and participants provided written informed consent, according to CARE guidelines and in compliance with the Declaration of Helsinki principles (*Clinicaltrials.gov*, *number*: *NCT04066816*).

Patient eligibility

Eligible healthy adults were referred to the Division of Gastroenterology for screening or surveillance colonoscopy by their primary physicians during their initial office consultation. A total of 47 male and female participants, ages 50 to 65 years, who had scheduled routine screening colonoscopies, underwent a screening process to ensure eligibility. Subjects were eligible if they met the following criteria: (i) not allergic to walnuts nor hypersensitive to tree nuts; (ii) not having a current active malignancy or previous history of GI malignancy; (iii) no current or previous history of ulcerative colitis or Crohn disease; (iv) did not use antibiotics within the past month prior to consenting; (v) have not been treated with steroids, immunosuppressive agents, or other anti-inflammatory drugs 1 week prior to starting intervention; and (vi) are willing to avoid foods and drinks that are high in ellagic acid for the entire trial. Exclusion criteria include (i) current active malignancy, previous history of GI malignancy, or altered GI anatomy; (ii) current evidence or previous history of ulcerative colitis or Crohn disease; (iii) HIV infection and chronic viral hepatitis; (iv) allergy to walnuts or hypersensitivity

to tree nuts; (v) use of antibiotics within the past month; (vi) individuals with blood coagulation disorder or on anticoagulant therapy; (vii) treated with steroids, immunosuppressive agents, or other anti-inflammatory drugs 1 week prior to starting intervention; (viii) non-English speaking patients who require an interpreter to give consent; (ix) patients residing in the department of correction; (x) inability to comply with the protocol requirements; and (xi) any other condition that, in the opinions of the principal investigator, might interfere with study objectives.

After the selection process, 47 people were enrolled in the study, as shown in Supplementary Fig. S1. Six of the 47 participants dropped out because of compliance difficulties, 2 dropped out because of a canceled colonoscopy related to COVID-19, and one was excluded from the statistical analysis because of not being able to obtain a blood sample. A total of 39 patients, 21 females and 18 males, age, 50 to 65 years, comprised the analytic study population. All participants signed a written informed consent before the start of the study and were free to withdraw at any time throughout the study with no obligation. All but one female patient provided a blood specimen (Supplementary Fig. S1).

Patient demographics and lifestyle factors

After consent, all participants had a complete history and physical examination and a review of past medical, surgical, and family history, including colon cancer. Clinical and demographic data were obtained during the office visit, including key elements of the patient's medical history, dietary supplements, and medications, including NSAIDs, smoking status, alcohol intake, physical fitness, and family history of colon polyps and cancer. Body mass index (BMI, kg/m^2) was calculated from weight (kg) and height (m) measurements obtained during the initial office consultation.

Participants completed a block food frequency questionnaire (BFFQ) 2014, a full-length questionnaire with 127 items to assess dietary behavior during the past 12 months, including information on foods high in ellagic acid, such as berries, walnuts or flax seeds, peanuts, sunflower seeds, other nuts, or seeds, to assess diet quality and dietary habits. These surveys were submitted to Quest Nutrition for data compilation. The average of caloric intake, nutrients, and daily food group consumption was also used for posterior analyses. These data were used to assess the subjects' dietary behavior. The informed consents, collection of clinical data, demographic data, and study protocols followed strict institutional guidelines. Study compliance was assessed by the levels of urinary creatinine-normalized urolithin A immediately following the 1-week run-in period. Urolithin levels at this point should be close to or at zero, assuming all ellagitannin-containing foods were properly avoided.

Endoscopic procedure and polyp collection

Colonoscopies were performed as part of routine health maintenance for screening or surveillance. Individuals underwent standard-of-practice medical care with a split-dose bowel preparation and colonoscopy using a high-definition colonoscope (16). Polyps were confirmed using the standardized endoscopy report (completed by the study endoscopists immediately following the procedure) and were included in the electronic medical record. One or more colon polyps were detected in 11 of 39 subjects, including one right-sided sessile serrated adenoma/polyp, two advanced adenomas, and more commonly detected hyperplastic polyps (Supplementary Fig. S2; Supplementary Table S2). All polyp tissues were sent to the Department of Pathology and processed by formalin-fixation, paraffin-embedding (FFPE). Histologic features of polyps were determined by Dr. M. Zenali.

Analysis of serum inflammatory markers

A measure of 5 mL whole-blood sample was collected from each subject on the morning of the colonoscopy, and serum was aliquoted and stored frozen at −80°C until use. Multiplex analysis of 73 cytokines, chemokines, and growth factors was performed using the Luminex 200 system by Eve Technologies as follows: Human Supplemental Biomarker 10-Plex Discovery Assay, Human Cytokine Panel A 3-Plex Discovery Assay, Human Cytokine 20-Plex Discovery Assay, Human Cardiovascular Disease Panel 3 9-Plex Discovery Assay, Human High Sensitivity 6-Plex Discovery Assay, Human Soluble Cytokine Receptor 14-Plex Discovery Assay, Human Serum Amyloid A & ADAMTS13 Discovery Assay, and Human Metabolic Hormone 9-Plex Discovery Assay (MilliporeSigma). The complete list is provided in Supplementary Table S3.

For the analysis of serum inflammatory markers, Spearman ρ statistics was used to estimate a rank-based measure of association (positive or negative correlation) of 73 log-transformed $[\log(1 + x)]$ serum biomarker values. Correlated pairs of markers were ranked using corr_cross function from the lares R package, and pairs were considered significant for P values <0.05. For analyzing the association of ordered (lowest to highest) urolithin A levels and blood serum biomarker levels across all patients, we fit a linear model with integrated smoothness estimation to the log-normalized $[\log(1 + x)]$ values of each individual biomarker related to the log-normalized $[\log(1 + x)]$ urolithin A values to obtain the correlation curves and error margins. For evaluating differential abundance trends for blood serum biomarkers between the three identified groups (low, medium, and high) or two groups (combined low and medium vs. high groups), two statistical tests were used, the t test using Welch–Satterthwaite approximation with 0.95 confidence interval and the Wilcoxon signed-rank test to evaluate the fold change of log-transformed values and P value significance. A heatmap analysis using the complexHeatmap R package for scaled and centered blood serum biomarker values was used to illustrate further trends in inflammatory markers in relation to urolithin A groups.

Analysis of peripheral blood mononuclear cells

Total human peripheral blood mononuclear cells (PBMC) were purchased from ATCC (PCS-800-011). PBMCs were cultured overnight in RPMI 1640 medium (ATCC 30-2001) supplemented with 10% FBS, 100 U/mL penicillin, and 100 U/mL streptomycin at 37°C and 5% CO_2. The cells were seeded into a 24-well plate (1×10^6 cells in 1 mL per well) with each group having three wells. The following day, varying concentrations of urolithin A (0, 3, 10, and 20 μmol/L) were added to the media, and the cells were incubated for 5 hours. Each condition also included a stimulated and unstimulated group, performed in triplicate. A measure of 10 ng/mL phorbol 12-myristate 13-acetate (PMA) and 1 μg/mL ionomycin were added to each well of the stimulated groups after urolithin A treatment, and all wells were cultured for 24 hours at 37°C, 5% CO_2. Conditioned media was then collected and stored at −80°C until analysis. The supernatant levels of TNFα were quantified by ELISA according to the manufacturer's protocol (BioLegend, Human ELISA MAX).

Metabolomic analysis in urine and feces

Urine samples were collected at the end of the 1-week run-in and prior to colonoscopy, ensuring dietary compliance and allowing sufficient depletion of systemic urolithin metabolites prior to walnut supplementation. Spot urine samples collected by patients were aliquoted and stored at −80°C within 24 hours of collection. As urolithins are primarily (~95%) excreted in the urine as glucuronides, and less so as sulfates, sulfoglucuronides, and diglucuronides (17, 18), the sample was subjected to overnight hydrolysis with arylsulfatase and ß-glucuronidase. The levels of nine urolithin metabolites, before and after hydrolysis, were measured by ultraperformance LC/MS-MS as described (19), using creatinine to standardize diuresis. Fecal samples were collected at the end of the 1-week run-in period and then following the 3-week walnut supplementation. Samples were stored at −80°C until processing for LC/MS-MS for quantitation of urolithin metabolites.

For analysis of urolithin A in fecal samples, a Vanquish UPLC (Thermo Fisher Scientific) was used for injecting samples for chromatographic separation using a C-18 chromatography column (50 × 2.1 mm Kinetex 1.7 μmol/L, C18, 100 Å; Phenomenex); 40°C column temperature; 0.4 mL/minute flow rate; mobile phase A: 99.9% water (Thermo Fisher Scientific, Optima LC/MS) and 0.1% formic acid (Thermo Fisher Scientific, Optima LC/MS); and mobile phase B: 99.9% acetonitrile (Thermo Fisher Scientific, Optima LC/MS) and 0.1% formic acid (Thermo Fisher Scientific, Optima LC/MS), with the following gradient: 0 to 0.5 minutes 5% B, 0.5 to 8 minutes 100% B, 8 to 9 minutes 100% B, 9.1 to 10 minutes 5% B, and 10 to 10.5 minutes 5% B. Mass spectrometry (MS) analysis in negative polarity mode was performed on an Orbitrap Exploris 480 (Thermo Fisher Scientific) mass spectrometer equipped with HESI-II probe sources. The following probe settings were used for both MS for flow aspiration and ionization: spray voltage of 2500 V, sheath gas (N_2) pressure of 35 psi, auxiliary gas pressure (N_2) of 10 psi, ion source temperature of 350°C, S-lens RF level of 50 Hz, and auxiliary gas heater temperature at 400°C.

Spectra were acquired in negative ion mode over a mass range of 75 to 1,450 m/z. An external calibration with Pierce LTQ Velos ESI Negative Ion Calibration Solution (Thermo Fisher Scientific) was performed prior to data acquisition with a ppm error of less than 1. Data were recorded with data-dependent MS/MS acquisition mode. Full scan at the MS1 level was performed with 30K resolution. MS2 scans were performed at 11,250 resolution with maximum IT time of 60 ms in profile mode. MS/MS precursor selection windows were set to m/z 1.5 with m/z 0.5 offset. MS/MS active exclusion parameter was set to 5.0 seconds. Quantification analysis for urolithin A was performed using Xcalibur software (Thermo Fisher Scientific).

IMC analysis of polyp tissue and IHC

Five-μm-thick serial sections were prepared from polyp FFPE blocks obtained from study participants, and IMC staining was performed at the JAX-UConn Single Cell Core. Sections were processed by Hyperion IMC and converted to mcd files for downstream analysis. We applied end-to-end computational analysis workflow for multiplexed image processing based upon an earlier publication (20), including an R code for metadata preprocessing and DeepCell for cell segmentation and the steinbock/ImcSegmentationPipeline framework for segmentation and quantification. Following "counts" data quantification analysis, SpatialExperiment and SC1 (21) tools were used for clustering analysis, differential expression analysis, and data visualization. Additionally, MCD Viewer and cytomapper tools were used for spatial visualization. Correlation analysis between delta fecal levels of urolithin A and IMC marker expression was done by averaging the expression levels of each region of interest (ROI) belonging to one sample and using Spearman correlation. Additional details about antibodies used for IMC, clustering analysis, and quantitation can be found in Supplementary Table S4.

IHC analysis of polyp tissue

IHC was used to validate the expression and localization of vimentin and CD163 within the colonic mucosa. FFPE polyp sections were deparaffinized and subjected to citrate-based antigen retrieval. Tissues were incubated overnight at 4°C with primary antibodies for vimentin (1:1,000, Cell Signaling Technology) and CD163 (1:2,000, Cell Signaling Technology) followed by 30-minute incubation with horseradish peroxidase–conjugated anti-rabbit secondary antibody (Cell Signaling Technology). Signals were detected using DAB substrate (Vector Laboratories) and counterstained with hematoxylin.

Statistical analysis

Urolithin metabolism data were clustered into three groups using a model-based, unbiased clustering analysis

based on parameterized finite Gaussian mixture models to stratify patients into distinct groups based on their urinary urolithin A levels. For analysis of serum inflammatory markers, Spearman ρ statistics was used to estimate a rank-based measure of association (positive or negative correlation) of 73 log-transformed [log(1 + x)] serum biomarker values. General characteristics, lifestyle factors, and dietary intake across tertiles of urolithin A production after walnut intervention, as well as case and control groups, were expressed as means and SD or SE for continuous variables and as numbers and percentages for categorical variables. To examine differences in sociodemographic or lifestyle characteristics across tertiles of urolithin A production after walnut intervention, one-way ANOVA was used for continuous variables and a χ^2 test was applied for categorical variables. Dietary intake across tertiles of urolithin A production after walnut intervention and case and control groups, was compared using analysis of covariance to adjust for sex, BMI, and alcohol consumption. Associations between ellagic acid intake and urolithin A levels after walnut intervention were calculated by logistic regression. *P* values were considered statistically significant at < 0.05.

Data availability

The datasets generated and/or analyzed during the current study are available from the corresponding author upon reasonable request.

Results

Demographics, macronutrient, and food group intake of study participants

The study group consisted of 39 patients who completed the entire study, including the high-definition colonoscopy performed at the completion of walnut supplementation. Study details are provided in Supplementary Fig. S1. A blood draw was not accomplished in one patient. Demographics of the study population (mean age 54 years) are shown in **Table 1**. Most of the population was Caucasian (82%), nonsmoking (98%), and distributed between male (45%) and female (55%). Thirty-three percent of patients were classified as obese, with a BMI ≥30, and approximately half (52%) consumed alcohol.

We further examined potential differences in adenoma risk between patients based on food group intake (**Table 2**). A polyp "risk score" was determined as "control" (none or low/medium-risk polyps) or high-risk (one or more advanced polyps). After adjusting for sex, BMI, and alcohol consumption, high total sugar and poultry intakes were significantly correlated with a greater risk of developing advanced polyps ($P = 0.022$ for total sugar intake; $P = 0.016$ for poultry intake; **Table 2**). Furthermore, lower calories (%) from monounsaturated fatty acids were trending toward significance in at-risk patients with a *P* value of 0.08. However, no significant trends were observed when correlating urolithin production with the polyp risk score (Supplementary Table S5).

Table 1. Demographics of the study population ($n = 39$).

Parameter	Mean ± SD or (*N*, %)
Age (years)	53.5 ± 4.0
Sex	
Male	18 (45%)
Female	22 (55%)
BMI (kg/m^2)	
Overall average BMI	28.4 ± 6.1
BMI <30	27 (67.5%)
BMI ≥30	13 (32.50%)
Race	
White	26 (65%)
Black	5 (12.5%)
Asian	8 (20%)
Hawaiian/Pacific Islander	1 (2.5%)
Ethnicity	
Hispanic/Latino	1 (2.5%)
Non-Hispanic/Latino	39 (97.5%)
Smoking	
Smoker	1 (2.5%)
Nonsmoker	39 (97.5%)
Alcohol	
Drinker	21 (52.5%)
Nondrinker	19 (47.5%)

Urolithin metabolism following walnut supplementation

The creatinine-normalized concentrations of a panel of nine urolithin metabolites (urolithin A, isourolithin A, urolithin B, urolithin C, urolithin D, urolithin E, urolithin M5, urolithin M6, and urolithin M7) were measured in the urine samples of our study group after enzymatic hydrolysis. These data are shown in Supplementary Table S6. As summarized in **Fig. 2A**, the most abundant species present are urolithin A and isourolithin A. Urolithin A metabolism data were then clustered into three groups using a model-based, unbiased clustering analysis based on parameterized finite Gaussian mixture models to stratify patients into distinct groups based on their urinary urolithin A levels (ng/mg creatinine-normalized), prior to and after walnut supplementation. There was a marked fold change (>25) between low- and high-producer means, with optimal stratification of urolithin A into three groups based upon mean and median values equal to 144.4, 2,792.1, and 20,656.2 ng/mg (low, medium, and high, respectively). Notably, mean values for the three groups, when the same stratification is applied to data prior to walnut supplementation, were 101.2, 120.2, and 74.2 ng/mg, respectively, showing no clear trend attributed to before walnut supplementation, further emphasizing the walnut-dependent effect.

In **Fig. 2B**, the creatinine-normalized urolithin values for all measured metabolites for each patient demonstrate highly variable urolithin production capacity within this study group. Differences before and after walnut supplementation were compared using the paired Wilcoxon signed-rank test, highlighting marked differences before and after walnut supplementation in isourolithin A ($P < 0.0001$), urolithin A

Table 2. Adjusted nutrient and food group intakes of study participants based on at-risk and control groups 1 and 2.

Nutrient intake	*n*	Control (*n* = 24), mean (SE)	Case (*n* = 14), mean (SE)	*P* value
Calories, kcal/day	38	1,255.4 (97.3)	1,349.8 (127.6)	0.561
Protein, g/day	38	49.7 (5.2)	57.2 (6.8)	0.382
Calories (%) from protein	38	15.7 (0.6)	16.4 (0.8)	0.534
Fat, g/day	38	56.9 (4.6)	55.4 (6.0)	0.848
Calories (%) from fat	38	40.9 (1.3)	37.5 (1.8)	0.132
Carbohydrate, g/day	38	134.8 (11.0)	155.4 (14.5)	0.267
Calories (%) from carbohydrate	38	43.3 (1.5)	46.3 (2.0)	0.237
Saturated fat, g/day	38	18.9 (1.7)	18.6 (2.2)	0.928
Calories (%) from saturated fat	38	13.7 (0.7)	12.8 (0.9)	0.433
Monounsaturated fatty acids, mg/day	38	22.4 (1.9)	20.7 (2.5)	0.592
Calories (%) from monounsaturated fatty acids	38	15.9 (0.6)	14.0 (0.8)	0.082
Polyunsaturated fatty acids, mg/day	38	11.0 (1.1)	11.3 (1.5)	0.871
Calories (%) from polyunsaturated fatty acids	38	8.1 (0.6)	7.5 (0.8)	0.621
Calories (%) from omega-3 fatty acid	38	0.9 (0.1)	0.9 (0.1)	0.977
Trans fat, g/day	38	1.4 (0.2)	1.5 (0.3)	0.842
Total fiber, g/day	38	13.9 (1.4)	15.0 (1.9)	0.644
Vitamin D intake (IU/day)	38	74.3 (11.4)	97.4 (14.9)	0.226
Vitamin C intake (mg/day)	38	92.5 (10.2)	82.6 (13.4)	0.559
Vitamin E intake (IU/day)	38	8.0 (0.6)	7.7 (0.9)	0.828
Vitamin B6, mg/day	38	1.3 (0.1)	1.5 (0.1)	0.225
Vitamin B9, μg/day	38	294.9 (25.8)	279.0 (33.9)	0.712
Vitamin B12, μg/day	38	2.4 (0.3)	3.2 (0.4)	0.152
Calcium, mg/day	38	506.1 (51.7)	618.3 (67.8)	0.197
Magnesium, mg/day	38	199.3 (17.0)	221.3 (22.3)	0.44
Iron, mg/day	38	9.1 (0.8)	9.1 (1.0)	0.997
Zinc, mg/day	38	6.7 (0.8)	7.9 (1.1)	0.361
Selenium, μg/day	38	65.4 (6.2)	66.7 (8.1)	0.9
Sodium, mg/day	38	1,641.1 (143.1)	1,604.7 (187.6)	0.878
Potassium, mg/day	38	1972.8 (159.0)	2,269.5 (208.5)	0.266
Total sugar, g/day	38	54.5 (5.3)	75.6 (7.0)	0.022
Alcohol, g/day	38	9.1 (3.9)	9.8 (5.1)	0.914
Food group intake				
Vegetables (servings/day)	38	3.5 (0.4)	3.3 (0.6)	0.801
Fruit and fruit juices (frequency/day)	38	1.1 (0.2)	1.4 (0.2)	0.249
Breads, cereals, rice, and pasta (servings/day)	38	3.0 (0.4)	2.6 (0.5)	0.47
Meat, fish, poultry, beans, and eggs (servings/day)	38	1.7 (0.2)	1.9 (0.3)	0.52
Meat (g/day)	38	15.5 (5.5)	19.0 (7.2)	0.706
Fish (g/day)	38	19.6 (4.8)	15.2 (6.3)	0.586
Poultry (g/day)	38	13.8 (4.7)	33.5 (6.2)	0.016
Beans (g/day)	38	23.9 (7.5)	29.4 (9.8)	0.656
Eggs (g/day)	38	26.7 (5.8)	31.1 (7.6)	0.655
Milk, yogurt, and cheese (servings/day)	38	0.8 (0.1)	1.1 (0.2)	0.178
Peanut butter (g/day)	38	7.4 (1.8)	5.7 (2.4)	0.581

($P < 0.0001$), and urolithin C ($P < 0.0001$). Using rank-based Spearman correlation as a means of quantifying potential urolithin interactions, we found that urolithin A and iso-urolithin A had the highest positive correlation ($R = 0.87$, $P < 0.0001$; **Fig. 2C**). These data are consistent with proposed interactions reported for the urolithin metabolic pathway. Indeed, the learned network graph (**Fig. 2D**) supports the connection of urolithin C with isourolithin A and urolithin A within this metabolic pathway, followed by the connection with isourolithin A and urolithin B. Interestingly, a strong positive correlation is also present between urolithin M7 and urolithin C. We performed a principal component analysis (PCA) using all measured metabolites (**Fig. 2E**). Within-group variability is lower in the low versus high urolithin A producers that was captured by the first two principal components.

Dietary intake of study participants based on urolithin A levels

Using the three-group stratification of patient groups, we analyzed the macronutrient intakes based on the BFFQ survey. After adjusting for covariates, high total fat ($P = 0.024$), polyunsaturated fatty acids ($P = 0.021$), and vitamin E ($P = 0.030$) intakes were significantly correlated with greater urinary urolithin A production after walnut intervention, whereas trending toward significance were

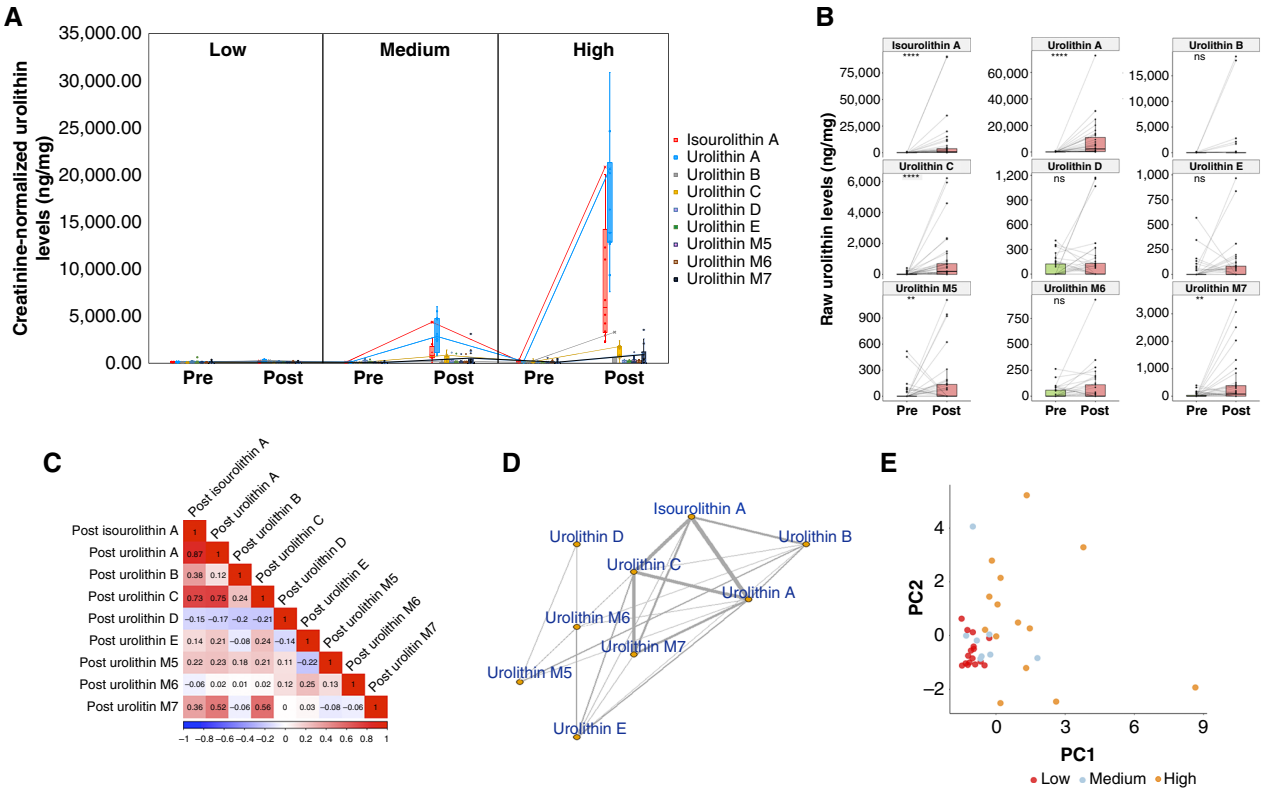

Figure 2.

Urolithin levels presented as model-based clustering and correlation analysis. **A,** Distribution of urolithin metabolites detected in the urine before (Pre) and after (Post) walnut consumption. Patients are stratified into three groups based on delta urolithin A levels (low, medium, and high). **B,** Creatinine-normalized urolithin levels (ng/mg) of each urolithin metabolite measured for each patient before and after walnut consumption. Paired Wilcoxon signed-rank significance codes: ****, <0.0001; ***, <0.0001–0.001; **, <0.001–0.01; ns, >0.05. **C,** Rank-based Spearman correlation between the individual urolithin metabolites. The strongest correlations can be observed in the urolithin A, isourolithin A, and urolithin C subgroups. **D,** Urolithin network graph (pathway) as learned from study cohort metabolomic data. The Spearman correlation score was used to create the adjacency matrix for the illustrated graph, in which vertices represent each of the measured urolithin metabolites and edges exist between nodes and vertices, in which the edge weight is ≥0.25 and the edge thickness represents the value of the correlation score. **E,** Three urolithin metabolism groups/clusters projected on the first two principal components (PC) of the complete urolithin (including all nine metabolites) dataset. The three groups are identified as low (red), medium (light blue), and high (orange) producers based on the delta urolithin A Gaussian mixture model clusters.

saturated fatty acids ($P = 0.07$), monounsaturated fatty acids ($P = 0.07$), sodium ($P = 0.09$), meat/fish/poultry/bean/egg ($P = 0.08$), and egg intakes ($P = 0.09$; Supplementary Table S7). Based on demographics and dietary data collected at baseline using the BFFQ, urinary urolithin A levels after walnut intervention were not associated with sociodemographic or lifestyle characteristics of the study participants (Supplementary Table S8).

Serum inflammatory marker analysis and correlation with urolithin A

A total of 73 inflammatory markers (Supplementary Table S3) were measured in the serum of 38 patients at the time of colonoscopy. A heatmap showing the average normalized levels of the most responsive serum inflammatory markers, clustered by the delta urolithin A metabolism, is shown in **Fig. 3A**. We compared these inflammatory markers in a pairwise correlation analysis of all measured markers (**Fig. 3B**). C-peptide had the highest pairwise correlation with leptin. sIL-6R correlated negatively with several proinflammatory cytokines and ILs that formed a tight cluster of significantly correlated pairs, with the most significant pairwise correlations including IL-23 with thyroid peroxidase (TPO; $R = 0.95$, $P < 0.0001$), IL-33 with TPO ($R = 0.95$, $P < 0.0001$), IL-33 with thymic stromal lymphopoietin (TSLP; $R = 0.93$, $P < 0.0001$), IL-23 with TSLP ($R = 0.91$, $P < 0.0001$), and TPO with TSLP ($R = 0.91$, $P < 0.0001$). Several additional pairs of inflammatory markers were significantly correlated, including IL-21 with LIF and IL-16 with insulin.

The relationship between serum inflammatory markers and urinary urolithin A levels (combining low and medium metabolic groups) was further stratified by obesity status, shown in violin plots (BMI ≥30; **Fig. 3C**). Eleven of 38 individuals were classified as obese, and within this group, higher urolithin A levels were significantly correlated with lower levels of soluble form of intracellular adhesion molecule 1 (sICAM-1; $P = 0.018$) and epithelial neutrophil–

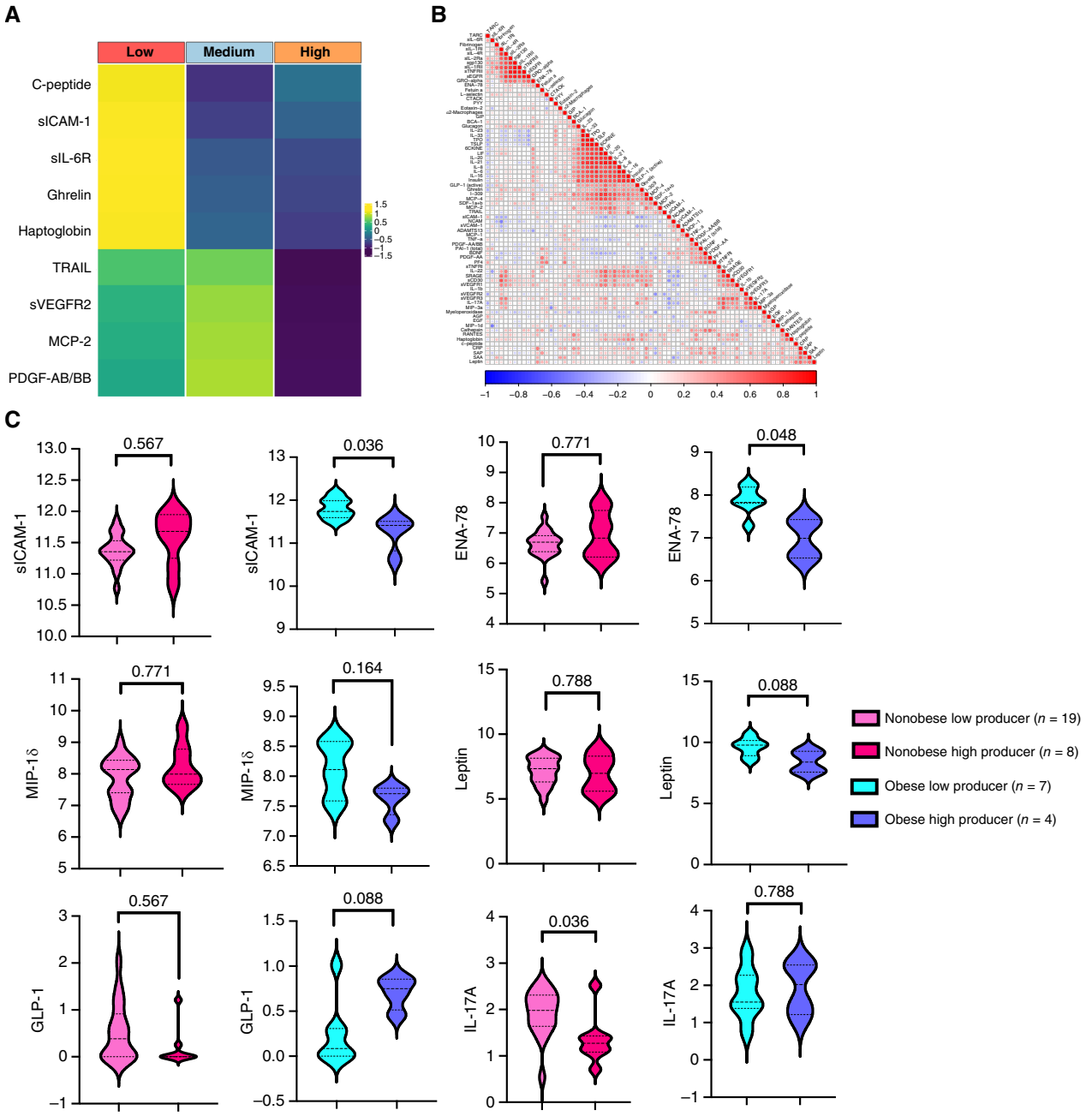

Figure 3.

Blood serum biomarkers and correlation with urolithin A levels. **A,** Heatmap showing the average normalized levels of log(1 + *x*)-transformed serum inflammatory markers, clustered by urolithin metabolic groups (low, medium, and high). C-peptide, sICAM-1, sIL-6R, ghrelin, and haptoglobin are each most lowered in the high–urolithin A producers. **B,** Pairwise rank-based Spearman correlation of serum inflammatory markers shows a total of 73 inflammatory markers that were measured in patient serum at the time of colonoscopy. **C,** Violin plots show four groups of high (red/blue) and low (pink/light blue) urolithin A producers, stratified by obese (BMI ≥30; $n = 12$) and nonobese (BMI <30; $n = 27$) subjects. Thick dotted lines indicate the median values, and thin dotted lines indicate upper and lower quartiles. We compared median serum marker levels between low and high urinary urolithin producers, stratified by obese and nonobese subjects. Among obese subjects, median serum inflammatory markers were generally lower for high producers, whereas this trend did not hold for nonobese subjects. Overall, FDR-adjusted *P* values indicate that these results were significant for sICAM-1 ($P = 0.036$), IL-17A ($P = 0.036$), and ENA-78 ($P = 0.048$). High and low/medium urolithin A producers were classified via Gaussian mixture model–based unbiased modeling, with a median value of 10,987.5 ng/mg for high producers and median value of 703.5 ng/mg for low/medium producers. One patient with a negative value (−144) needed to be assigned a zero value because of log-transformation requirements. All serum markers are reported as ln(x), except for GLP-1 that was log-transformed using ln(x + 1).

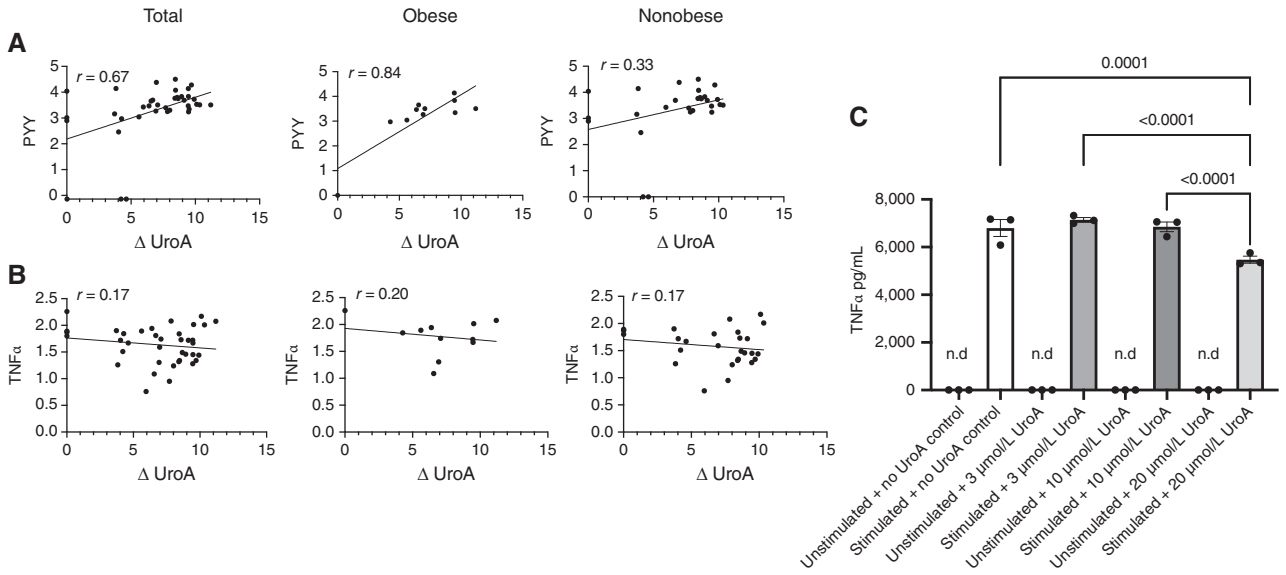

Figure 4.

Examples of positive and negative correlations of selected inflammatory markers with urinary urolithin A levels. **A,** Peptide YY shows a significant positive correlation with urolithin A (UroA) levels ($P = 0.003$) in all patients and in BMI-high ($P = 0.001$) subjects and trending in BMI-normal ($P = 0.087$) subjects, (**B**) whereas TNFα shows a trend toward a negative, nonsignificant correlation in both groups. **C,** Effects of urolithin A on TNFα secretion in ionomycin/PMA-stimulated PBMCs. Urolithin A (3, 10, and 20 μmol/L) was preincubated for 5 hours with PBMCs, followed by 24-hour stimulation with ionomycin/PMA, as described under "Materials and Methods." Samples were incubated in triplicate, and data were analyzed by one-way ANOVA, followed by Bonferroni for multiple comparisons (mean ± SEM). n.d, not detected; PYY, peptide YY.

activating peptide 78 (ENA-78; $P = 0.029$). IL-17a was significantly negatively correlated ($P = 0.0094$) with urolithin A in the normal BMI group. The levels of leptin and macrophage inflammatory protein 1δ (MIP-1δ) trended lower in the high-BMI, high–urolithin A group, although the changes did not reach significance ($P = 0.07$ and 0.16, respectively; **Fig. 3C**). Interestingly, the posttranslational product of proglucagon glucagon-like peptide 1 (GLP-1) was highest in the high-BMI, high–urolithin A group, although not reaching significance ($P = 0.07$).

As shown in **Fig. 4A**, we next examined how serum inflammatory markers may correlate with individual urolithin A levels across the entire patient group. Interestingly, peptide YY, associated with inhibition of colorectal cancer (22), was positively correlated with increasing levels of urolithin A, particularly in BMI-high subjects ($R = 0.70$; $P = 0.001$). On the other hand, TNFα levels trended lower in normal weight and high-BMI individuals, although the P values did not reach statistical significance (**Fig. 4B**). Finally, we tested the expression levels of several inflammatory cytokines produced *in vitro* by ionomycin/PMA-stimulated PBMCs. Although the secretion of TNFα was significantly elevated in stimulated PBMCs, preincubation with 20 μmol/L urolithin A for 5 hours was found to reduce TNFα secretion by up to 20% (6,799.3 ± 357.1 vs. 5,469.5 ± 144.1), measured at 24 hours (**Fig. 4C**).

IMC analysis of colon polyps

To gain additional insights into how urolithin A may affect colonic health, a multiplex analysis of polyp tissues was undertaken using high-dimensional imaging. As noted above, one or more colon polyps were detected in 11 of 39 subjects (Supplementary Table S2). IMC was used to examine the spatial distribution of epithelial cells and stromal composition of the TME within and adjacent to colon polyps and how these cellular profiles depend upon urolithin formation. A full description of the IMC computational workflow is described in **Fig. 5**. Polyp sections included 23 ROIs, prepared from colons of low and high urolithin A producers shown in Supplementary Fig. S2. Each polyp biopsy contained a mixture of neoplastic regions and normal-adjacent mucosa.

A heatmap showing normalized IMC marker values per ROI for urolithin-low/high and polyp/normal (top) is shown in **Fig. 6A**, demonstrating expression differences between the urolithin groups. Notably, several differentially expressed proteins were significantly reduced in the urolithin A–high group, including vimentin (0.24-fold; $P < 0.0001$) and CD163 (0.51-fold; $P < 0.0001$; **Fig. 6B**). Conversely, CD90 and podoplanin levels were increased in the urolithin-high group.

Vimentin levels per ROI are represented as violin plots, highlighting the marked difference in expression between urolithin-low and -high ROIs (**Fig. 6C**). To determine whether fecal levels of urolithin A may directly affect IMC markers within polyps, nonhydrolyzed ("free") urolithin A was measured in the feces of the highest and lowest urinary urolithin A tertiles (Supplementary Table S9) using LC/MS-MS. First, we show that fecal urolithin A levels are significantly ($P < 0.001$; $R = 0.82$) correlated with total urinary (hydrolyzed) levels (Supplementary Fig. S3). Next, fecal

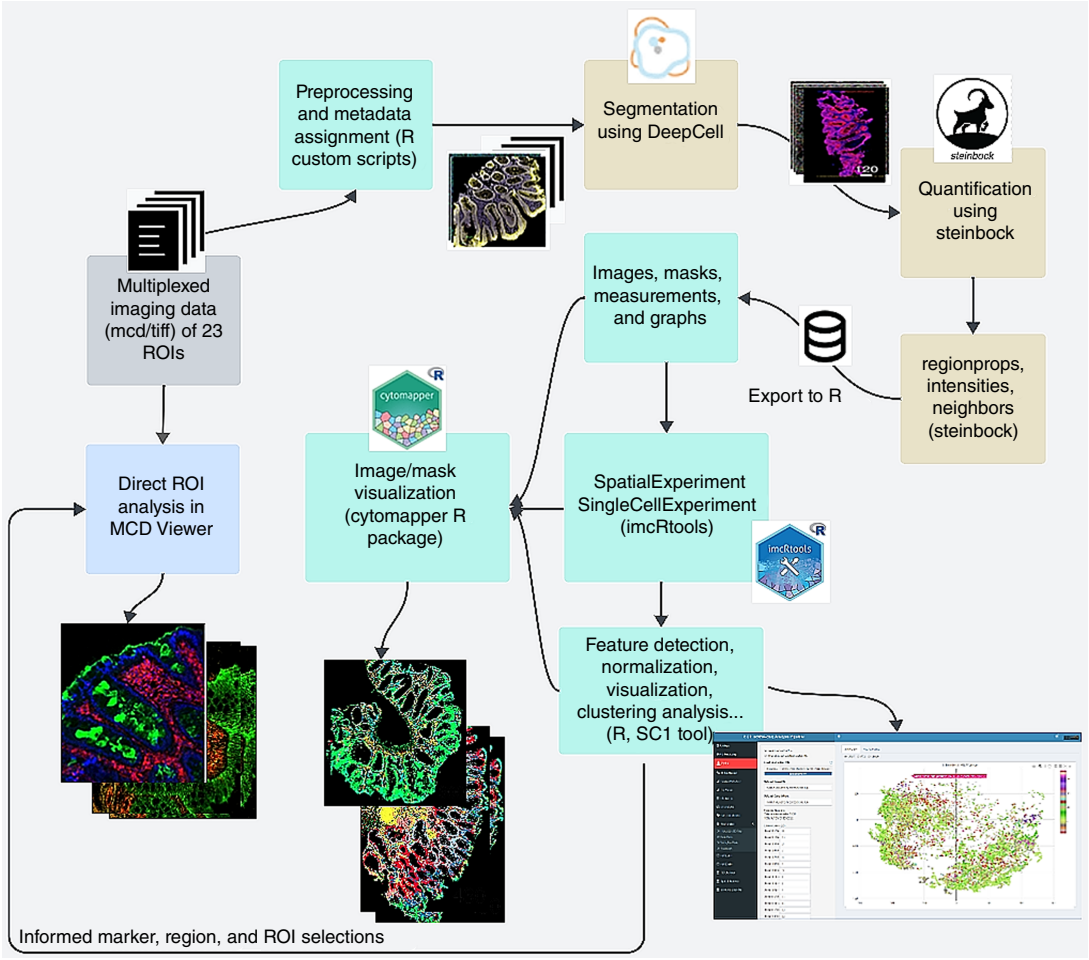

Figure 5.
IMC computational analysis workflow. Schema shows the IMC assay and computational analysis workflow. End-to-end workflow for multiplexed image processing and analysis components. The pipeline includes custom code, DeepCell for segmentation, steinbock for quantification, MCD Viewer and cytomapper for visualization, and SpatialExperiment and SC1 tools for clustering analysis, differential expression analysis, and visualization. (Created using Lucidchart.com.)

levels were correlated with IMC markers using Spearman correlation. Interestingly, vimentin and CD163 showed a strong negative correlation with fecal urolithin A levels ($R = -0.75$ and $R = -0.71$, respectively; **Fig. 6D**), indicating for the first time that the localized release of urolithin A from gut microbial metabolism has a direct effect on colon tissues. IMC images show vimentin intensity between the urolithin-low and -high ROIs. In **Fig. 6E**, selected MCD Viewer images demonstrate the stromal density of vimentin in selected ROIs. To confirm these findings, IHC was used to validate the expression and localization of vimentin and CD163 within the colonic mucosa. Vimentin staining [**Fig. 6F** (left)] was evident within the mucosa of a serrated polyp biopsied from a urolithin-low producer and markedly reduced within the stroma of a tubular adenoma from a urolithin-high producer. In addition, CD163 staining was more intense in a urolithin A–high producer relative to a low producer [**Fig. 6F** (right)].

Unsupervised clustering of ROIs was then used to identify distinct cell populations within polyps. A total of 14 groups were merged into seven individual clusters. A heatmap showing maximum-scaled mean marker expression across all ROIs per cluster is shown in **Fig. 7A**. The hierarchical clustering dendrogram identifies two main subclusters: two epithelial clusters (left, blue) showing expression of epithelial markers EPCAM/e-cadherin and pan-cytokeratin and five nonepithelial clusters (right, pink) populated by stromal, muscle layer, antigen-presenting cells (APC), myeloid lineage, and lymphocytes, including T and B cells (lymphocytes). The number of cells comprising each cluster is indicated. Epithelia were differentiated into nonproliferating and proliferating clusters based on Ki-67 expression. Stromal clusters include a "muscle layer," denoted by strong expression of the endothelial markers CD31 and α-SMA and collagen I. APCs showed high

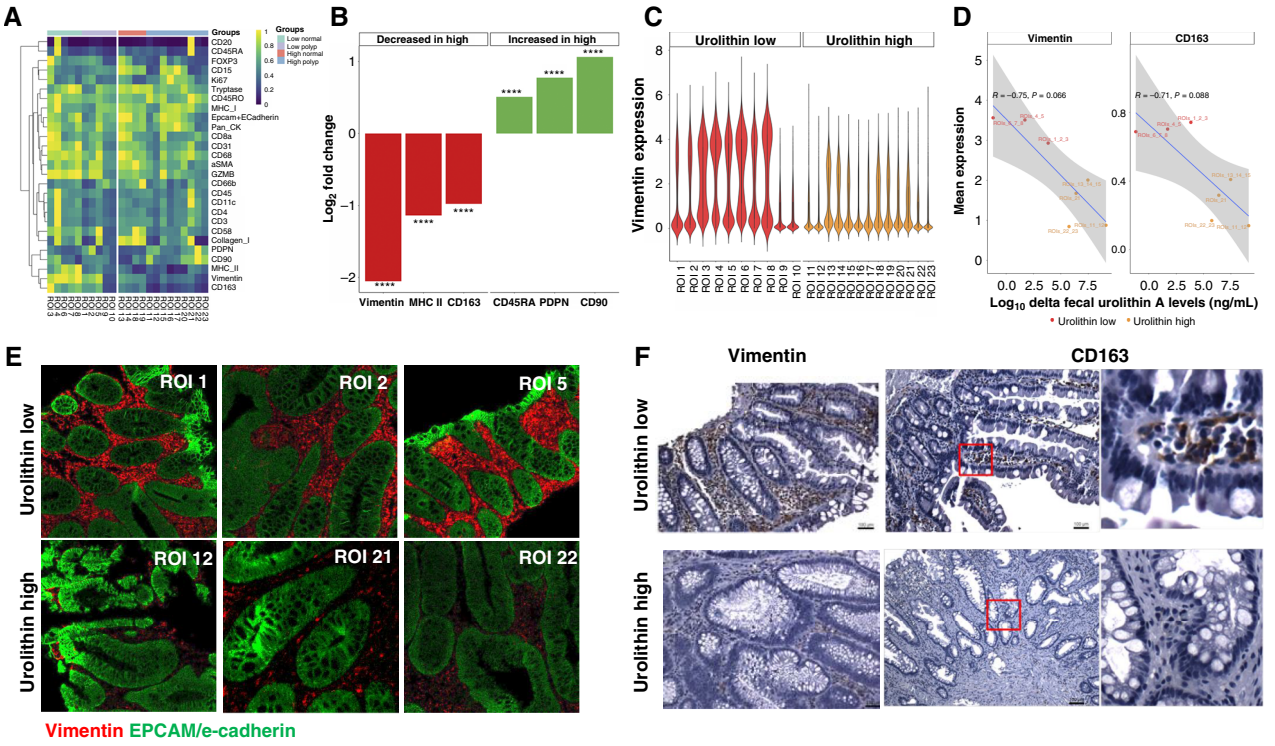

Figure 6.

IMC analysis of polyps. **A,** Heatmap of averaged expression of each measured marker for each ROI, stratified by urolithin low and high, normal and polyp tissues. **B,** A total of six markers were found to be differentially expressed between the groups, including vimentin (>−4-fold). Significance codes: ****, <0.0001; ns, >0.05. **C,** Violin plots of vimentin expression are shown. Expression values were obtained by transforming the raw IMC counts with the inverse hyperbolic sine function (typical of cytometry data). **D,** Correlations between log delta fecal urolithin A levels for the top and bottom tertiles of the sample group and mean expression levels of vimentin and CD163. **E,** Representative IMC images of urolithin low and high, highlighting the marked reduction of vimentin in urolithin high. IMC images were visualized using MCD Viewer. **F,** IHC analysis of vimentin expression in urolithin low (ROI 5, serrated) vs. high (ROI 22, tubular) adenomas. Images were captured using conventional microscopy and QCapture software.

expression of CD66b (neutrophils), CD68, CD163 (macrophage), CD11c (dendritic cells), and vimentin. A "myeloid lineage" cluster showed overlapping expression patterns to APCs, with elevated tryptase and granzyme B (mast cells and NK cells). "Stromal" was categorized by the broad expression of numerous nonepithelial markers but lacking EPCAM/e-cadherin and pan-cytokeratin. The lymphocyte cluster showed expression of lymphocyte markers, notably CD20 and CD3, indicating co-localization of these two distinct lineages.

Figure 7B shows a PCA plot of centered log ratios of phenotype proportions across all ROIs. These data highlight the degree of similarity between tissues based on their phenotypic proportions. Overall, urolithin-low and -high tended to segregate from one another, with urolithin-low polyps showing a more disperse spread. To further validate the cluster phenotypes and elucidate their biological significance, a compositional bar plot indicating the percentage of cells belonging to each cluster for each individual ROI, stratified by urolithin-low and -high levels, in normal versus polyp is shown (**Fig. 7C**). Viewing the overall composition of each tissue explains some of the trends observed in the PCA. Urolithin-low ROIs (normal and polyp) consistently showed higher prevalence of the vimentin containing an APC cluster. Notably, this cluster was markedly reduced in urolithin-high polyps, whereas the lymphocyte cluster was more prevalent. To better visualize phenotypic composition, all seven clusters were projected onto the segmentation mask of two urolithin-high polyps [**Fig. 7D** (left)]. Based on the intense localization of the lymphocyte cluster, we examined the presence and distribution of lymphocyte markers (CD8a, CD3, CD20, and EPCAM/e-cadherin) on these tissues using MCD Viewer (**Fig. 7D**). Co-localization of these markers is likely due to the presence of a lymphoid aggregate, underscored by the $CD20^+$ pocket surrounded by a $CD3^+$ crown, possibly indicating a tertiary lymphoid structure (23).

Discussion

Diet can influence cancer risk. Plant-derived compounds common in many foods, such as polyphenols, have antioxidant and cancer-preventive properties (1). Ellagic acid is a nonflavonoid polyphenol derived from the hydrolysis of ellagitannins, and foods high in content of this polyphenol,

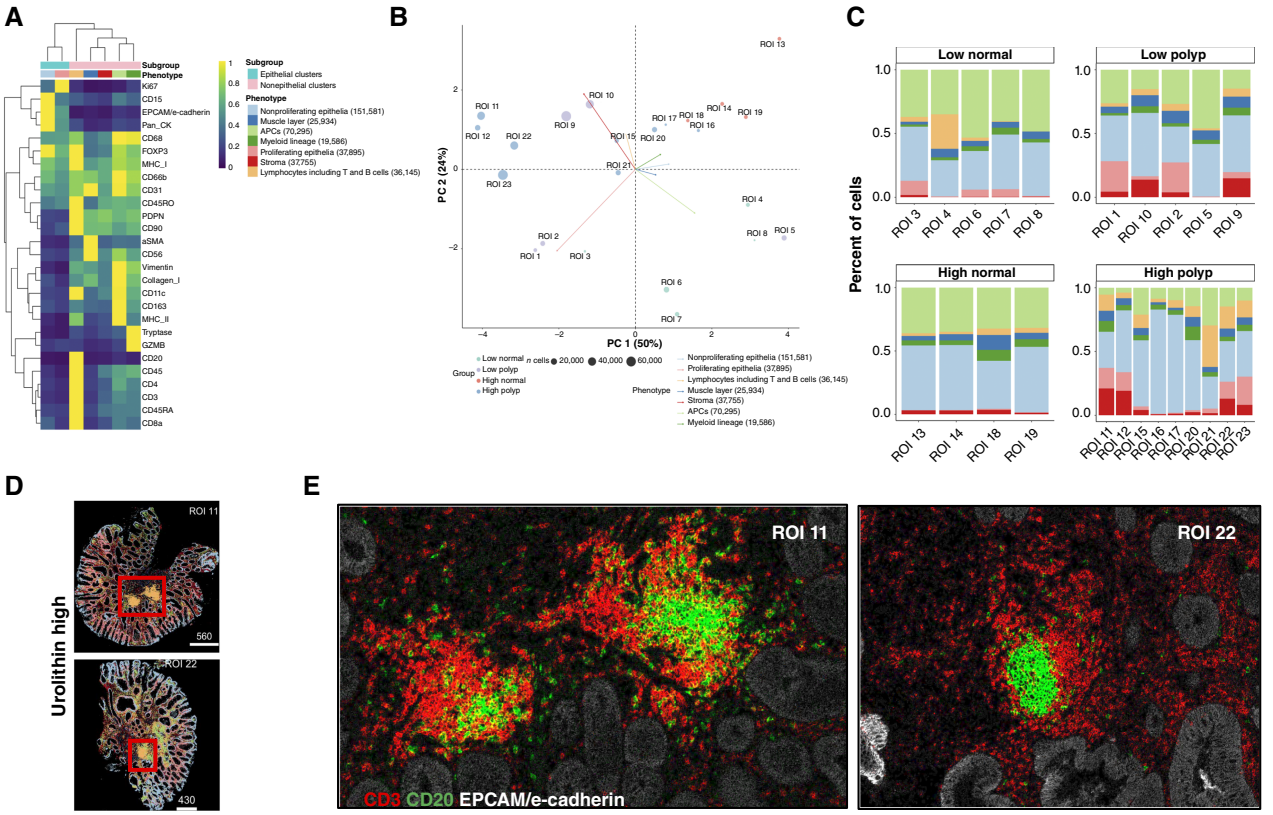

Figure 7.

Unsupervised clustering analysis. **A,** Cluster analysis heatmap showing maximum-scaled mean marker expression across all ROIs per cluster showing heterogeneous cell types and distinct tissue co-localization. Hierarchical clustering shows two epithelial clusters and five nonepithelial clusters. **B,** PCA of centered log ratios of phenotype proportions across the ROIs. A segregation of urolithin-low and -high groups can be visualized. PC, principal component. **C,** Compositional bar plots showing the percentage of cells belonging to each cluster for each individual ROI, stratified by low and high, normal and polyp tissues, clearly highlight an increase in vimentin-containing APC cluster. **D,** Projections of phenotype clusters onto two urolithin-high ROIs using segmentation masks are shown, highlighting the dense localization of the lymphocytes including T and B cells (lymphocytes; boxed). **E,** Corresponding IMC images of CD3, CD20, and EPCAM/e-cadherin to show that dense lymphocyte aggregation could be due to the formation of lymphoid structures.

such as berries, pomegranate juice, and walnuts, have shown anti-inflammatory properties (7, 9, 24, 25). Walnuts contain a complex array of nutrients that may have additive and/or synergistic properties that contribute to reduced cancer risk (26–29). Walnuts are a rich source of polyunsaturated fatty acids (eicosapentaenoic acid and docosahexaenoic acid), tocopherols, antioxidant polyphenols, and active prebiotics, including fiber (27). Independent of the direct effect of these constituents, walnuts can influence the structure of microbial communities and the abundance of microbes that produce beneficial metabolites (e.g., short-chain fatty acids) or affect inflammatory processes (13, 15). Even a 3-day consumption of walnuts modulates the gut microbiota, while increasing SCFAs (30). Overall, these findings highlight the health benefits of walnuts and their role in luminal gut metabolism in study participants that are representative of the general population living in the Farmington Valley of central Connecticut (Supplementary Table S10). The present study has investigated the effects of walnut supplementation on a panel of systemic inflammatory markers and the spatial architecture of the TME in a local population. Dietary supplementation with walnut enhances urolithin formation and is inversely correlated with the levels of several inflammatory markers. As anticipated from earlier clinical studies (3), we found significant interindividual differences in urolithin formation, both in urine and fecal streams. These differences are likely due to individual microbial composition, and future studies will address these differences within this study group.

Our recent review describes the health benefits of walnuts (31). Rajaram and colleagues (32) build an evidence base for effects of tree nuts on inflammatory markers. Cross-sectional data from the Nurses' Health Study and the Health Professional's Follow-Up Study demonstrated higher tree nut consumption is associated with lower levels of C-reactive protein (CRP) and IL-6, although meta-analysis of nine randomized controlled trials failed to show a significant effect on CRP [reviewed (33)]. Our results also did not find a significant effect of urolithin A on serum CRP (all patients: $P = 0.41$, $R = 0.14$; obese patients: $P = 0.86$, $R = 0.06$,

nonobese patients: $P = 0.12$, $R = 0.31$). However, longer walnut supplementation (2 years) in the WAHA study (34) reported significantly reduced levels of several inflammatory markers, including E-selectin, IL-6, TNFα, IFN-γ, GMCF, and IL-1β. However, these clinical trials did not associate urolithin A formation with serum biomarkers, as performed in our trial. When we compared the levels of 73 inflammatory markers stratified by urolithin A, several significant changes were identified, including an inverse association with sICAM-1 and ENA-78, which were highest in the low–urolithin A group (**Fig. 3A**, red). In addition, TRAIL, sVEGFR2, MCP-2, and platelet-derived growth factor were progressively reduced in the medium and high (orange) urolithin A groups (**Fig. 3A**). These data suggest that even short-term ingestion of walnut can have beneficial effects on systemic inflammation.

Previous studies have shown that dietary polyphenols can modulate lipid and glucose metabolism (35). Based on prior studies indicating that ellagic acid can attenuate obesity and obesity-related complications (1), we investigated the relationship between serum markers and urolithin A formation (combining low and medium groups), stratified by obesity status (**Fig. 3C**). Within this group, urolithin A levels were significantly correlated with lower levels of sICAM-1 and ENA-78, although GLP-1, leptin, and MIP-1δ each trended in this direction in obese individuals. A similar, significant reduction was also found for serum levels of IL-17A, although this effect was restricted to nonobese patients (**Fig. 3C**). The secretable sICAM-1 has been proposed as a biomarker for several forms of cancer, including colon cancer (36). ENA-78, also known as CXCL5, is a potent chemoattractant for neutrophils that is elevated in response to inflammatory cytokines, including IL-1 and TNFα, and has been proposed as a potential marker for colorectal cancer (37). Elevated levels of MIP-1δ (CCL15) were found to be associated with increased colorectal cancer risk (38). GLP-1, produced by posttranslational processing of proglucagon, has anti-inflammatory properties and contributes to overall gut health (39). Interestingly, the levels of GLP-1 were highest in the high-BMI, high–urolithin A group. This is the first report indicating that walnut may elevate GLP-1, warranting further study. Interestingly, the levels of peptide YY were significantly elevated by serum urolithin A concentrations in both obese and nonobese subjects, a potentially important effect of walnut consumption on gut health (22). Lastly, although serum levels of TNF α only trended lower with increasing urolithin A levels, our *in vitro* experiments establish a potentially protective role of urolithin A in PBMCs (**Fig. 4**), an effect that may have translational relevance. Overall, our findings indicate that even short-term intake of walnut ellagitannins may be associated with improved inflammatory profiles, especially within obese subjects.

During the past decade, our understanding of the TME has been enhanced by the development of high-dimensional spatial imaging, providing a detailed view of direct cellular interactions within tumor tissue. We have used IMC to examine the cellular composition of colonic polyps and to determine whether urolithin formation may directly affect the spatial composition of a select group of immune-related markers. When we combined spatial imaging of the TME with clustering analysis of segmented single-cell data, seven clusters were identified, showing heterogeneous cell types with distinct tissue co-localization (**Figs. 6** and **7**). The heatmap and compositional bar plot identify clusters that differ significantly between low- and high-urolithin groups. These include a nonspecific immune cell cluster that is projected onto several polyps (**Fig. 7**). This cluster is localized to lymphoid structures that are more prominent in the urolithin-high group (4/13 vs. 2/10 polyp and adjacent normal tissues, respectively, in the high- versus low groups). Future studies will be undertaken to examine potential mechanisms associated with urolithins that contribute to these immunogenic effects.

The effects of urolithin A on differential expression of CD163 and vimentin may have clinical relevance. Several recent articles describe the association of CD163-positive M2 macrophages in colorectal cancer pathogenesis, including effects on cell migration and lymph node metastasis (40–42). In fact, urolithin A was recently reported to remodel the stromal immune microenvironment in a mouse pancreas cancer model, while attenuating immunosuppressive M2-like macrophages (43). These *in vivo* findings have been validated in cell culture. In a recent study comparing urolithin B and isourolithin A (free and glucuronidated) with urolithin A (44), the nonconjugated form of urolithin A was the most active ellagic acid metabolite with respect to lipopolysaccharide-induced inhibition of the inflammatory response in THP-1–derived macrophages, RAW 264.7 macrophages, and PBMC-derived macrophages. Thus, our findings in polyp tissue suggest a potential beneficial role for urolithin A in attenuating this subpopulation of immunosuppressive macrophages, even in early stages of colonic neoplasia, and further studies are warranted. Vimentin is associated with tumor progression and malignancy in colorectal cancer (45). Our findings that urolithin A reduces vimentin expression in polyp tissue was not unexpected. Recent reports indicate the effects of this polyphenol on epithelial–mesenchymal transition with reduced vimentin expression in several cancer types, including lung, glioblastoma, and nasopharyngeal cancer cells (46–48). Mechanistically, vimentin promoter activity is enhanced by AP-1 binding activity (49). In macrophage culture, urolithin A suppresses lipopolysaccharide-induced AP-1 activation, thereby suppressing proinflammatory mediators and formation of reactive oxygen (50). Thus, it is possible that urolithin A formed by luminal microbial metabolism is absorbed directly by colonic mucosa and prior to phase II conjugation, directly affects AP-1 transcriptional targets, including vimentin. As urolithin A, but not the glucuronide conjugates, have anti-inflammatory properties (44), our demonstration that fecal levels of "free" urolithin A are negatively correlated with both vimentin and CD163 (**Fig. 6D**) lends additional support for a direct effect on colonic mucosa.

In summary, although gut microbial metabolism of food-derived ellagitannins is correlated with cardiovascular disease

risk (51, 52), urolithin metabolism and its relationship with colorectal cancer risk has not previously been evaluated. The present study has incorporated personalized nutrition within the context of colonic health, while focusing on the consequences to a panel of serum inflammatory markers that are significantly differentiated based on urolithin A formation. As noted earlier, urolithins affect numerous cell signaling pathways relevant to cancer, and the imaging analysis of colon polyps has uncovered differentially expressed proteins that may be directly influenced by urolithin A. Overall, the possibility that walnuts given to healthy volunteers improve colonic health and potentially lowers colorectal cancer risk factors associated with urolithin A has been tested. This trial substantiates the functional benefits of walnuts and establishes the molecular consequences of interindividual variability in urolithin A formation, both in the urine and fecal streams, validating the concept that ellagitannin-rich foods play an important role in the diet.

Authors' Disclosures

A. Aksenov reports being a co-founder of Arome Science, Inc. and Bileomix, Inc. V.N. Motta reports other support from Standard BioTools during the conduct of the study, as well as other support from Standard BioTools outside the submitted work. No disclosures were reported by the other authors.

Authors' Contributions

M.R. Moussa: Data curation, software, formal analysis, methodology, writing–original draft, writing–review and editing. **N. Fan:** Data curation, methodology, writing–original draft, project administration, writing–review and editing. **J. Birk:** Resources, supervision, investigation, methodology, project administration, writing–review and editing, colonoscopies. **A.A. Provatas:** Data curation, validation, methodology, writing–review and editing. **P. Mehta:** Software, formal analysis, validation. **Y. Hatano:** Software, formal analysis, investigation, visualization, methodology. **O.K. Chun:** Data curation, methodology. **M. Darooghegi Mofrad:** Data curation, methodology. **A. Lotfi:** Data curation, methodology, writing–review and editing. **A. Aksenov:** Data curation, methodology. **V.N. Motta:** Data curation, software. **M. Zenali:** Resources, formal analysis. **H. Vaziri:** Colonoscopies. **J.J. Grady:** Formal analysis, statistics. **M. Nakanishi:** Data curation, formal analysis, validation, visualization. **D.W. Rosenberg:** Conceptualization, resources, data curation, software, formal analysis, supervision, funding acquisition, validation, investigation, visualization, methodology, writing–original draft, project administration, writing–review and editing.

Acknowledgments

This study was supported by generous funding from the American Institute for Cancer Research /California Walnut Commission award #586610 for D.W. Rosenberg, California Walnut Commission award #AG2021 for D.W. Rosenberg, NCI award #CA270079 for M.R. Moussa, NCI award #CA252045 for D.W. Rosenberg, and the National Science Foundation award #2341725 for M.R. Moussa. We would like to thank Margaret Toro for her dedicated assistance with patient enrollment. We are also gratefully indebted to Amy Pallotti for her invaluable contribution to protocol development and study administration. We also express immense gratitude toward our Advanced Practice Registered Nurse, Heidi L. Rose, Fatima Osmanovic, Allison M. Rinaldi, and Kendra Damon-Smith, for their dedication and support toward our ongoing NIH study.

Note

Supplementary data for this article are available at Cancer Prevention Research Online (http://cancerprevres.aacrjournals.org/).

Received August 20, 2024; revised December 5, 2024; accepted February 21, 2025; published first February 25, 2025.

References

1. Kang I, Buckner T, Shay NF, Gu L, Chung S. Improvements in metabolic health with consumption of ellagic acid and subsequent conversion into urolithins: evidence and mechanisms. Adv Nutr 2016;7:961–72.
2. Selma MV, Beltrán D, Luna MC, Romo-Vaquero M, García-Villalba R, Mira A, et al. Isolation of human intestinal bacteria capable of producing the bioactive metabolite isourolithin A from ellagic acid. Front Microbiol 2017;8:1521.
3. García-Villalba R, Giménez-Bastida JA, Cortés-Martín A, Ávila-Gálvez MÁ, Tomás-Barberán FA, Selma MV, et al. Urolithins: a comprehensive update on their metabolism, bioactivity, and associated gut microbiota. Mol Nutr Food Res 2022;66:e2101019.
4. Ginefra P, Hope HC, Chiang Y-H, Nutten S, Blum S, Coukos G, et al. Urolithin-A promotes $CD8^+$ T cell-mediated cancer immunosurveillance via FOXO1 activation. Cancer Res Commun 2024;4:1189–98.
5. Denk D, Petrocelli V, Conche C, Drachsler M, Ziegler PK, Braun A, et al. Expansion of T memory stem cells with superior anti-tumor immunity by Urolithin A-induced mitophagy. Immunity 2022;55:2059–73.e8.
6. Nakanishi M, Chen Y, Qendro V, Miyamoto S, Weinstock E, Weinstock GM, et al. Effects of walnut consumption on colon carcinogenesis and microbial community structure. Cancer Prev Res (Phila) 2016;9:692–703.
7. Guan F, Tabrizian T, Novaj A, Nakanishi M, Rosenberg DW, Huffman DM. Dietary walnuts protect against obesity-driven intestinal stem cell decline and tumorigenesis. Front Nutr 2018;5:37.
8. Nakanishi M, Matz A, Klemashevich C, Rosenberg DW. Dietary walnut supplementation alters mucosal metabolite profiles during DSS-induced colonic ulceration. Nutrients 2019;11:1118.
9. Chen Y, Nakanishi M, Bautista EJ, Qendro V, Sodergren E, Rosenberg DW, et al. Colon cancer prevention with walnuts: a longitudinal study in mice from the perspective of a gut enterotype-like cluster. Cancer Prev Res (Phila) 2020;13:15–24.
10. Hintze KJ, Benninghoff AD, Ward RE. Formulation of the Total Western Diet (TWD) as a basal diet for rodent cancer studies. J Agric Food Chem 2012;60:6736–42.
11. Baxter NT, Zackular JP, Chen GY, Schloss PD. Structure of the gut microbiome following colonization with human feces determines colonic tumor burden. Microbiome 2014;2:20.
12. Lipińska L, Klewicka E, Sójka M. The structure, occurrence and biological activity of ellagitannins: a general review. Acta Sci Pol Technol Aliment 2014;13:289–99.
13. Bamberger C, Rossmeier A, Lechner K, Wu L, Waldmann E, Fischer S, et al. A walnut-enriched diet affects gut microbiome in healthy caucasian subjects: a randomized, controlled trial. Nutrients 2018;10:244.

14. Baer DJ, Gebauer SK, Novotny JA. Walnuts consumed by healthy adults provide less available energy than predicted by the atwater factors. J Nutr 2016;146:9–13.
15. Holscher HD, Guetterman HM, Swanson KS, An R, Matthan NR, Lichtenstein AH, et al. Walnut consumption alters the gastrointestinal microbiota, microbially derived secondary bile acids, and health markers in healthy adults: a randomized controlled trial. J Nutr 2018;148:861–7.
16. Drew DA, Devers TJ, O'Brien MJ, Horelik NA, Levine J, Rosenberg DW. HD chromoendoscopy coupled with DNA mass spectrometry profiling identifies somatic mutations in microdissected human proximal aberrant crypt foci. Mol Cancer Res 2014;12:823–9.
17. Piwowarski JP, Stanisławska I, Granica S., Stefańska J, Kiss AK. Phase II conjugates of urolithins isolated from human urine and potential role of β-glucuronidases in their disposition. Drug Metab Dispos 2017;45:657–65.
18. Nuñez-Sánchez MA, García-Villalba R, Monedero-Saiz T., García-Talavera NV, Gómez-Sánchez MB, Sánchez-Álvarez C, et al. Targeted metabolic profiling of pomegranate polyphenols and urolithins in plasma, urine and colon tissues from colorectal cancer patients. Mol Nutr Food Res 2014;58:1199–211.
19. Provatas AA, Ayers SA, Callas AA, Birk JW, Lacson TA, Rosenberg DW. Quantitative determination of selected urolthin metabolites in human urine by simple sample preparation and UPLC-MS/MS analysis. Curr Top Anal Chem 2021;13:60–80.
20. Windhager J, Zanotelli VRT, Schulz D, Meyer L, Daniel M, Bodenmiller B, et al. An end-to-end workflow for multiplexed image processing and analysis. Nat Protoc 2023;18:3565–613.
21. Moussa M, Măndoiu II. SC1: a tool for interactive web-based single-cell RNA-Seq data analysis. J Comput Biol 2021;28:820–41.
22. Jing F, Liu G, Zhang R, Xue W, Lin J, Zhu H, et al. PYY modulates the tumorigenesis and progression of colorectal cancer unveiled by proteomics. Am J Cancer Res 2022;12:5500–15.
23. Le Rochais M, Hémon P, Ben-Guigui D, Garaud S, Le Dantec C, Pers J-O, et al. Deciphering the maturation of tertiary lymphoid structures in cancer and inflammatory diseases of the digestive tract using imaging mass cytometry. Front Immunol 2023;14:1147480.
24. Banerjee N, Kim H, Talcott S, Mertens-Talcott S. Pomegranate polyphenolics suppressed azoxymethane-induced colorectal aberrant crypt foci and inflammation: possible role of miR-126/VCAM-1 and miR-126/PI3K/AKT/mTOR. Carcinogenesis 2013;34:2814–22.
25. Umesalma S, Sudhandiran G. Differential inhibitory effects of the polyphenol ellagic acid on inflammatory mediators NF-kappaB, iNOS, COX-2, TNF-alpha, and IL-6 in 1,2-dimethylhydrazine-induced rat colon carcinogenesis. Basic Clin Pharmacol Toxicol 2010;107:650–5.
26. Nagel JM, Brinkoetter M, Magkos F, Liu X, Chamberland JP, Shah S, et al. Dietary walnuts inhibit colorectal cancer growth in mice by suppressing angiogenesis. Nutrition 2012;28:67–75.
27. Hardman WE. Walnuts have potential for cancer prevention and treatment in mice. J Nutr 2014;144(Suppl 4):555S–60S.
28. Vanden Heuvel JP, Belda BJ, Hannon DB, Kris-Etherton PM, Grieger JA, Zhang J, et al. Mechanistic examination of walnuts in prevention of breast cancer. Nutr Cancer 2012;64:1078–86.
29. Davis PA, Vasu VT, Gohil K, Kim H, Khan IH, Cross CE, et al. A high-fat diet containing whole walnuts (Juglans regia) reduces tumour size and growth along with plasma insulin-like growth factor 1 in the transgenic adenocarcinoma of the mouse prostate model. Br J Nutr 2012;108:1764–72.
30. Cortés-Martín A, Selma MV, Espín JC, García-Villalba R. The human metabolism of nuts proanthocyanidins does not reveal urinary metabolites consistent with distinctive gut microbiota metabotypes. Mol Nutr Food Res 2019;63:e1800819.
31. Fan N, Fusco JL, Rosenberg DW. Antioxidant and anti-inflammatory properties of walnut constituents: focus on personalized cancer prevention and the microbiome. Antioxidants (Basel) 2023;12:982.
32. Rajaram S, Damasceno NRT, Braga RAM, Martinez R, Kris-Etherton P, Sala-Vila A. Effect of nuts on markers of inflammation and oxidative stress: a narrative review. Nutrients 2023;15:1099.
33. Mateş L, Popa D-S, Rusu ME, Fizeşan I, Leucuţa D. Walnut intake interventions targeting biomarkers of metabolic syndrome and inflammation in middle-aged and older adults: a systematic review and meta-analysis of randomized controlled trials. Antioxidants (Basel) 2022;11:1412.
34. Cofán M, Rajaram S, Sala-Vila A, Valls-Pedret C, Serra-Mir M, Roth I, et al. Effects of 2-year walnut-supplemented diet on inflammatory biomarkers. J Am Coll Cardiol 2020;76:2282–4.
35. Amiot MJ, Riva C, Vinet A. Effects of dietary polyphenols on metabolic syndrome features in humans: a systematic review. Obes Rev 2016;17:573–86.
36. Benedicto A, Romayor I, Arteta B. Role of liver ICAM-1 in metastasis. Oncol Lett 2017;14:3883–92.
37. Yildirim K, Colak E, Aktimur R, Gun S, Taskin MH, Nigdelioglu A, et al. Clinical value of CXCL5 for determining of colorectal cancer. Asian Pac J Cancer Prev 2018;19:2481–4.
38. Song M, Sasazuki S, Camargo MC, Shimazu T, Charvat H, Yamaji T, et al. Circulating inflammatory markers and colorectal cancer risk: a prospective case-cohort study in Japan. Int J Cancer 2018;143:2767–76.
39. Mehdi SF, Pusapati S, Anwar MS, Lohana D, Kumar P, Nandula SA, et al. Glucagon-like peptide-1: a multi-faceted anti-inflammatory agent. Front Immunol 2023;14:1148209.
40. Lan J, Sun L, Xu F, Liu L, Hu F, Song D, et al. M2 macrophage-derived exosomes promote cell migration and invasion in colon cancer. Cancer Res 2019;79:146–58.
41. Min AKT, Mimura K, Nakajima S, Okayama H, Saito K, Sakamoto W, et al. Therapeutic potential of anti-VEGF receptor 2 therapy targeting for M2-tumor-associated macrophages in colorectal cancer. Cancer Immunol Immunother 2021;70:289–98.
42. Kim H-D, Kim SY, Kim J, Kim JE, Hong YS, Han B, et al. Dynamic increase of M2 macrophages is associated with disease progression of colorectal cancers following cetuximab-based treatment. Sci Rep 2022;12:1678.
43. Mehra S, Garrido VT, Dosch AR, Lamichhane P, Srinivasan S, Singh SP, et al. Remodeling of stromal immune microenvironment by urolithin A improves survival with immune checkpoint blockade in pancreatic cancer. Cancer Res Commun 2023;3:1224–36.
44. Bobowska A, Granica S, Filipek A, Melzig MF, Moeslinger T, Zentek J, et al. Comparative studies of urolithins and their phase II metabolites on macrophage and neutrophil functions. Eur J Nutr 2021;60:1957–72.
45. Ngan CY, Yamamoto H, Seshimo I, Tsujino T, Man-i M, Ikeda J-I, et al. Quantitative evaluation of vimentin expression in tumour stroma of colorectal cancer. Br J Cancer 2007;96:986–92.
46. Cheng F, Dou J, Zhang Y, Wang X, Wei H, Zhang Z, et al. Urolithin A inhibits epithelial-mesenchymal transition in lung cancer cells via P53-Mdm2-Snail pathway. Onco Targets Ther 2021;14:3199–208.
47. Shen C-K, Huang B-R, Charoensaensuk V, Yang L-Y, Tsai C-F, Liu Y-S, et al. Inhibitory effects of urolithins, bioactive gut metabolites from natural polyphenols, against glioblastoma progression. Nutrients 2023;15:4854.
48. Yang Y, Ren Z-Z, Wei W-J, He Z-L, Deng Y-L, Wang Z, et al. Study on the biological mechanism of urolithin a on nasopharyngeal carcinoma in vitro. Pharm Biol 2022;60:1566–77.
49. Wang Y, Wang J, Yang C, Wang Y, Liu J, Shi Z, et al. A study of the correlation between M2 macrophages and lymph node metastasis of colorectal carcinoma. World J Surg Oncol 2021;19:91.

50. Komatsu W, Kishi H, Yagasaki K, Ohhira S. Urolithin A attenuates pro-inflammatory mediator production by suppressing PI3-K/Akt/NF-κB and JNK/AP-1 signaling pathways in lipopolysaccharide-stimulated RAW264 macrophages: possible involvement of NADPH oxidase-derived reactive oxygen species. Eur J Pharmacol 2018;833:411–24.
51. Tindall AM, McLimans CJ, Petersen KS, Kris-Etherton PM, Lamendella R. Walnuts and vegetable oils containing oleic acid differentially affect the gut microbiota and associations with cardiovascular risk factors: follow-up of a randomized, controlled, feeding trial in adults at risk for cardiovascular disease. J Nutr 2020;150:806–17.
52. Selma MV, González-Sarrías A, Salas-Salvadó J, Andrés-Lacueva C, Alasalvar C., Örem A, et al. The gut microbiota metabolism of pomegranate or walnut ellagitannins yields two urolithin-metabotypes that correlate with cardiometabolic risk biomarkers: comparison between normoweight, overweight-obesity and metabolic syndrome. Clin Nutr 2018;37:897–905.